Kinetic phase diagram for island nucleation and growth during homoepitaxy

P. A. Mulheran[1] and M. Basham[2]
[1]*Department of Chemical and Process Engineering, University of Strathclyde, James Weir Building, 75 Montrose Street, Glasgow G1 1XJ, United Kingdom*
[2]*Department of Physics, University of Reading, Whiteknights, Reading RG6 6AF, United Kingdom*
(Received 29 May 2007; revised manuscript received 27 November 2007; published 26 February 2008)

The impact of small-island dissociation and mobility on island nucleation and growth during vapor deposition of thin films is analyzed using mean field rate equations. The dominant island nucleation and growth mechanism is mapped onto a temperature/deposition-rate kinetic phase diagram, using Cu(100) homoepitaxy as an example. The methodology provides analytical expressions for the boundaries on the diagram and encourages a deeper understanding of the growth mechanisms. A kinetic Monte Carlo simulation incorporating the small-island dynamics is also presented and used to test the kinetic phase diagram, and satisfactory agreement is found throughout.

DOI: 10.1103/PhysRevB.77.075427 PACS number(s): 68.35.Fx, 82.20.Wt, 68.55.−a, 81.15.Aa

The nucleation and growth of islands during thin film vapor deposition has received much attention over recent years.[1] Islands form the fundamental building blocks for crystalline nanostructures and multilayers, which find increasing utility in technology.[2] The mechanisms of island nucleation and growth provide many theoretical and modeling challenges.[3] The arrays of islands observed during or after submonolayer deposition often display scale invariant features through the size distribution or spatial organization.[4] Many simple Monte Carlo simulations reproduce these effects and have led to theoretical advances in understanding the phenomenon.[5–10] Of particular interest is that the way the island density, size, and spatial distribution varies with growth rate or temperature, and how this reflects the nucleation and growth mechanisms.[11–18] In particular, the critical island size, above which a small island tends to grow rather than dissociate, and the mobility of small islands are known to impact the statistical properties of the resulting island arrays.[10,14–17]

Calculating the dynamics of small islands during thin film growth over the relevant experimental time scales up to seconds presents a considerable modeling challenge.[20–28] Recently, we developed a self-learning kinetic Monte Carlo simulation powered by saddle-point searches to investigate the dynamics of small Cu/Cu(100) islands of sizes 2–8.[3,21,22] The simulation revealed the dynamic pathways for the small-island diffusion and dissociation through monomer release, along with the activation energies and frequency prefactors which we give here in Table I. Having obtained these data, it is desirable to be able to predict which mechanism, diffusion or island stability, and the dynamics of which size of island, will dominate the island nucleation and growth for a given growth temperature and deposition rate. In our earlier work, we performed a limited analysis of the numerical results from a set of mean field rate equations to produce a kinetic phase diagram to do this.

In this paper, we revisit this issue of how to make the kinetic phase diagram, using the data presented in Table I as an example. We improve on our previous work by focusing on analytic expressions for the regime boundaries, and correcting an oversight in our previous work concerning the mobility-dominated regime.[3] In addition, we provide some tests of our kinetic phase diagram using a Monte Carlo simulation of island nucleation and growth. We start with a description of this simulation and show some island arrays it produces, before we present our rate equation analysis and kinetic phase diagram.

Island nucleation and growth are simulated using a lattice-based kinetic Monte Carlo (kMC) procedure similar to that used previously by one of us.[14] Monomers are deposited randomly onto an initially bare substrate represented by a mesh at the rate F, which is the number of monolayers per second. Islands of size $s=2$ nucleate when monomers collide either through nearest-neighbor hopping (diffusion) or direct impacts from the deposition process. Islands of size $s<9$ are represented by points on the lattice (as are monomers) and they can diffuse and dissociate at the rates set by the growth temperature T and the kinetic parameters in Table I. This point-island approximation for these small islands is justified in the limit of low island densities, since capture rates depend on the ratio of diameter to interisland separation as Venables and others have shown.[11] Islands grow when another small island or monomer hops onto them, or through

TABLE I. Small-island diffusion and dissociation energies and prefactors used in this study. (Ref. 3).

Island size	Diffusion prefactor (10^{12} s^{-1})	Diffusion activation energy (eV)	Dissociation prefactor (10^{12} s^{-1})	Dissociation activation energy (eV)
1	5.25	0.536	⋯	⋯
2	3.75	0.513	24	0.904
3	5.25	0.614	32	0.929
4	15.0	0.717	1200	1.283
5	0.85	0.541	20	0.921
6	13.0	0.717	82	0.929
7	0.53	0.504	140	1.001
8	0.45	0.609	22	0.858

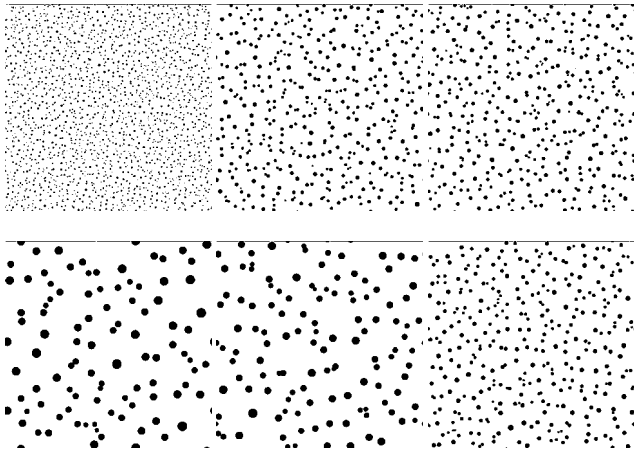

FIG. 1. Snapshots at 10% coverage of the island arrays grown during the simulation at $T=300$ K (top row) and $T=600$ K (bottom row) on a 2000×2000 lattice. In all cases, the ratio of deposition to monomer diffusion rate is 2×10^8 (the deposition rates are 2.65×10^{-5} and 0.83 ML/s, respectively). The middle image in both rows is for the full simulation with both small-island mobility and dissociation active; the left-hand images are with dissociation only active, and the right-hand images are for mobility only active.

direct hits by deposited monomers. Islands of size $s>8$ are stable and immobile, and maintain a circular footprint on the lattice occupying their size s sites. In the later stages of growth, neighboring circular islands can start to overlap; however, for the sake of simplicity these islands do not coalesce but remain as independent entities. Terminating the growth at modest (10%) substrate coverage, which we will do here, yields very little coalescence.

In Fig. 1, typical island arrays grown in the simulation are shown, at two different growth temperatures $T=300$ K (middle top) and $T=600$ K (middle bottom). In both cases, the ratio $R=D_1/F=2\times10^8$, so that in the absence of small-island dynamics, both would produce the same arrays of islands in a statistical sense. The impact of the small-island dynamics is therefore obvious. To distinguish which mechanism might dominate, we repeat the simulations firstly without allowing any small-island mobility (left-hand images) and then without allowing small-island dissociation (right-hand images). It is now apparent from the island densities in the images that at the lower temperature $T=300$ K in the top row, small-island mobility is a dominant process. In contrast, in the higher temperature simulation, small-island dissociation is the key and the mobility appears rather unimportant. As we will see below, the simulation at 300 K is, in fact, in the regime where dimer mobility dominates the scaling behavior, whereas the one at 600 K is dominated by critical island size $i=3$ behavior.

We now turn to a mean field rate equation description of the island nucleation and growth process, and follow Bartelt *et al.*[19] in analyzing competing rates to yield our kinetic phase diagram. The equation for the evolution of the monomer density n_1 can be expressed as

$$\frac{dn_1}{dt} \cong F - D_1 n_1 N - \left\{ \sum_{j=1}^{8} n_j + N \right\} + \left\{ \sum_{j=2}^{8} K_j n_j (1+\delta_{2,j}) - \sum_{j=2}^{8} n_1 n_j (D_1 + D_j) \right\}. \quad (1)$$

Here, the monomer diffusion rate is D_1, small islands of size $j<9$ diffuse at D_j and dissociate at the rate K_j, n_j is the density of island size $j<9$, and N is the density of stable islands of size $s>8$.

In writing Eq. (1), we are already making several approximations. We are working in a point-island limit for the monomer and small-island capture rates. This is a well-established approximation, which is justified at small coverage where islands themselves are small, and which has successfully yielded the scaling behavior with R,[6,7] which is our primary concern here. We also neglect the capture numbers $O(1)$ and their size dependence, an approximation originating from early work in this approach.[11] Finally, we are making a mean field assumption, in that we are neglecting environment-dependent contributions to individual island growth rates, and in doing so we cannot hope to obtain accurate island size distributions from these equations. However, this approach has a long pedigree of success for average quantities such as island densities, and previous work has shown how this form of rate equation captures many essential features of the nucleation and growth processes and the associated growth exponents.[29]

We wish to analyze Eq. (1) to decide which terms dominate the evolution of the island density. Amar *et al.*[7] have classified the evolution of the island density into four main regimes: Low-coverage where $n1<N$, intermediate where $N>n1$, aggregation where N has saturated, and coalescence where the stable islands grow into one another and merge (this starts to be important at about 40% coverage). We are interested in the intermediate regime, where the nucleation rates dictate the final island density and its scaling properties, and which occurs between coverage of about 0.001 and 0.1.[7] We shall, therefore, analyze the rate equation at the start of the intermediate regime at $\theta=Ft\sim0.001$, and test the scaling of the island density at the end of this regime at $\theta=0.1$.

The first braces $\{\}$ on the right of Eq. (1) represent direct hits onto existing point islands and monomers. At $\theta=0.001$, this term is negligible. In the second braces $\{\}$, we have terms representing monomer creation from the dissociation of small islands, and the adsorption of monomers by small islands of size $s<9$ through diffusion. Here, we are focusing on the regime where the density of large stable islands $N>n_j$. Then the terms in the second braces can also be neglected and we only need to consider monomer capture by the large islands represented by the second term on the right of Eq. (1). We thus find in the steady state regime of nucleation and growth,[19]

$$n_1 \approx \frac{F}{D_1 N}. \quad (2)$$

We can write similar expressions to Eq. (1) for the growth rate of n_j and N. The key to deciding which terms are im-

portant is to compare competing rates; however, to do this, we must have an expression for N that reflects the dominant growth mechanism. We, therefore, start by considering a regime of growth with a critical island size i, which occurs when islands of size $s>i$ grow faster than they dissociate or diffuse into neighbors, whereas smaller islands tend to dissociate rather than grow:

$$\frac{dN}{dt} \approx D_1 n_1 n_i, \tag{3}$$

and

$$\frac{dn_i}{dt} \approx D_1 n_1 n_{i-1} - K_i n_i \approx 0.$$

Recursively, using similar expressions for smaller islands down to size 2 and using Eq. (2), we find

$$n_i \approx D_1 n_1 \frac{n_{i-1}}{K_i} \approx \frac{F^i}{D_1 N^i \prod_{j=2}^{i} K_j}.$$

Combining with Eq. (3), we obtain

$$N \approx \left(\frac{\theta F^i}{D_1 \prod_{j=2}^{i} K_j} \right)^{1/(2+i)} \tag{4}$$

The expression in Eq. (4) reproduces the well-known growth exponent for the island density dependence on deposition flux F.[30] For the case $i=1$, the product in the denominator of Eq. (4) is replaced by 1. From our discussion above, we will take $\theta=0.001$ as a representative coverage at the start of the intermediate regime of nucleation.

Consider now the early stages of nucleation and growth. For sufficiently low deposition rates, the average time between monomer capture is such that all island dissociation mechanisms operate, and so we anticipate $i=8$. At higher deposition rates, the island and monomer densities will grow sufficiently large to allow other mechanisms to dominate. By comparing the rates of the competing mechanisms, we can predict when $i=8$ behavior with its associated island density [from Eq. (4)] no longer holds. Lower critical island size i occurs when islands of size $s=i+1$ no longer dissociate before they grow, i.e.,

$$n_{i+1} K_{i+1} \leq D_1 n_1 n_{i+1}.$$

From Eq. (2), we find

$$F \geq K_{i+1} N$$

and from Eq. (4) (with $i=8$ therein), we conclude

$$\log F \geq 5 \log K_{i+1} + \frac{1}{2} \log \theta - \frac{1}{2} \log D_1 - \sum_{j=2}^{8} \frac{1}{2} \log K_j. \tag{5}$$

The inequalities of Eq. (5) are plotted in Fig. 2(a) as a function of growth temperature T, using the data in Table I. It is apparent that the transition from $i=8$ to $i=3$ occurs at the lowest deposition rate for all experimentally relevant temperatures. The emergence of $i=3$ as a dominant growth mode is perhaps obvious from the symmetry of the Cu(100) surface and associated stability of tetramer ($s=4$) islands on this surface, evident from the high $s=4$ activation energy for dissociation in Table I.

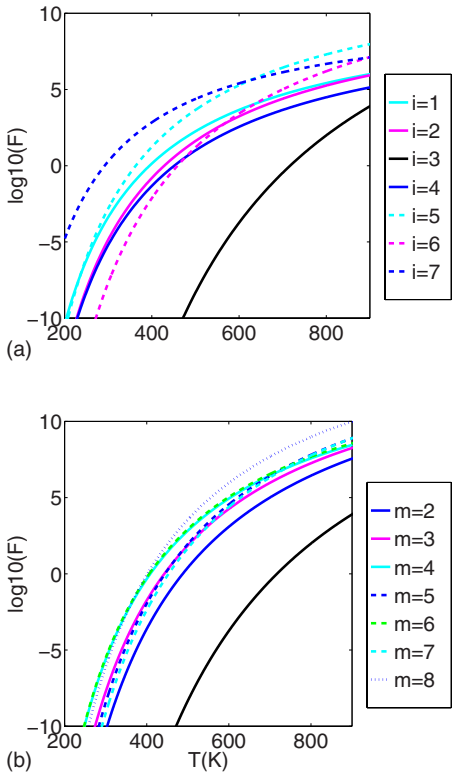

FIG. 2. (Color online) Boundaries between $i=8$ behavior and (a) lower-i regimes; (b) mobility regimes. The new regimes can occur above the lines. In (b), the black solid line is the boundary between $i=8$ and $i=3$ from (a).

The alternative mechanism due to the island mobility also needs to be considered. If the fate of a small island of size $m<8$ is determined by coalescence with existing stable islands of density $N \gg n_j$, then

$$D_m N \geq D_1 n_1,$$

yielding

$$\log F \geq -\frac{5}{3} \log D_m - \frac{1}{3} \log \theta + \frac{1}{3} \log D_1 + \sum_{j=2}^{8} \frac{1}{3} \log K_j. \tag{6}$$

The inequalities of Eq. (6) are plotted in Fig. 2(b), where we reproduce the $i=8$ to $i=3$ inequality for comparison. We conclude that the latter transition occurs at the lowest deposition rate.

We now turn to address the question of what other regimes exist at higher deposition rates. These are not immediately apparent from the plots of Fig. 2 which have been made using the island density at $i=8$ in the inequalities (5) and (6). Instead, we must consider the emergence of dominant growth mechanisms in a dynamical sense. When growth

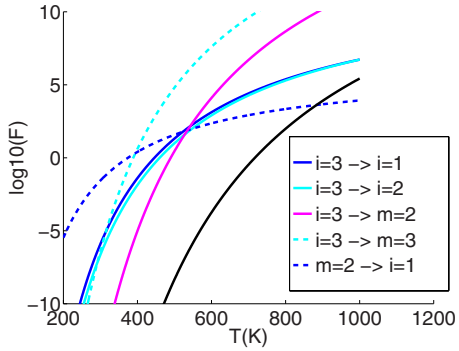

FIG. 3. (Color online) Boundaries between the $i=3$ regime and a lower critical island size or a mobility-dominated regime, where the new regimes can occur above the lines. The threshold for the dimer-mobility regime giving way to critical island size $i=1$ is also shown. The black solid line is the boundary between $i=8$ and $i=3$ from Fig. 2.

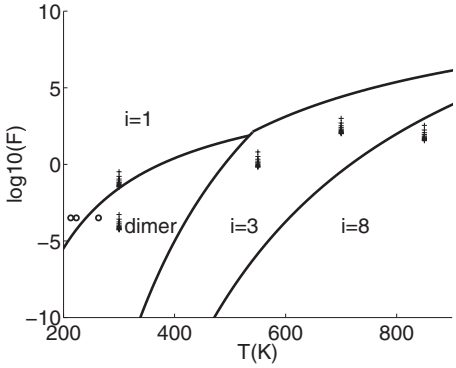

FIG. 4. The kinetic phase diagram deduced from Fig. 3. The dominant nucleation mechanism is indicated in each region of the diagram. The (T,F) points+are used to test the diagram with the Monte Carlo simulation. The circles are points from Ref. 31, as discussed in the text.

starts, the island density is necessarily very low implying $i=8$ behavior. As we have seen, as the island density grows, $i=3$ behavior takes over (at high deposition rate), since islands of size $s=4$ are now sufficiently stable and the monomer density sufficiently high. At even higher deposition rates, the island density grows higher still and transitions away from $i=3$ behavior to alternative regimes are possible and can be tested by using similar expressions to those given in Eqs. (5) and (6) but derived from the $i=3$ island density expression from Eq. (4). Hence, a transition to $i=1,2$ behavior occurs when

$$F \geq \frac{5}{2}\log K_{i+1} + \frac{1}{2}\log\theta - \frac{1}{2}\log D_1 - \sum_{j=2}^{3}\frac{1}{2}\log K_j. \quad (7)$$

Similarly, a transition to a dimer or trimer $(m=2,3)$ mobility-dominated regime occurs when

$$\log F \geq -5\log D_m - 2\log\theta + 2\log D_1 + \sum_{j=2}^{3} 2K_j. \quad (8)$$

The right-hand sides of the inequalities (7) and (8) are plotted in Fig. 3. It can be seen that at higher temperature $T>535$ K, $i=1$ behavior dominates at high deposition rate, whereas at lower temperature a dimer-mobility $(m=2)$ dominated regime occurs at high deposition rate. To complete our analysis, we must, therefore, consider how the island density N varies with flux in this regime, and whether $i=1$ behavior is possible at still higher values of flux F. Here, we can directly follow the arguments of Bartelt *et al.*,[19] setting the dimer density to the steady state and deducing the stable island nucleation rate,

$$\frac{dn_2}{dt} \approx D_1 n_1^2 - D_2 n_2 N \approx 0$$

and

$$\frac{dN}{dt} \approx D_1 n_1 n_2 \approx \frac{F^3}{D_1 D_2 N^4},$$

so that

$$N \approx \left(\frac{\theta F^2}{D_1 D_2}\right)^{1/5}. \quad (9)$$

We now determine the threshold for the $m=2$ to $i=1$ transition as

$$\log F \geq 3\log D_2 + 2\log\theta - 2\log D_1. \quad (10)$$

The right-hand side of the inequality (10) is also plotted in Fig. 3. As expected, even at low temperatures, when the deposition rate is sufficiently high, we recover $i=1$ behavior; once formed, a dimer is then more likely to meet another monomer and hence grow than diffuse into another island.

The curves of Fig. 3, along with the sense of the inequalities, map out the regions where we expect the island nucleation and growth to be dominated by the various mechanisms. The information is summarized in Fig. 4, which is our kinetic phase diagram for Cu(100) homoepitaxy. We also show the various test points we take on the diagram to validate its utility, as explained below. For each temperature T, we select a range of deposition rates F for use in our kMC simulation. The deposition-rate ranges span an order of magnitude. The range is limited by practical considerations for the memory requirements and execution time of the simulation.

For each (T,F) test point, we perform 100 runs of the Monte Carlo simulation described earlier, and measure how the stable island density N at 10% coverage varies with the deposition rate. By this stage, the dominant nucleation mechanism of the intermediate regime will dictate the scaling properties of the island density. The results are presented on log-log axes in Fig. 5, where the gradient through the respective set of points reveal the growth exponent. From Eq. (4), we predict growth exponents of $i/(2+i)$ for the critical island size behavior, while from Eq. (9), we predict an exponent $\frac{2}{5}$ for the dimer-mobility regime.

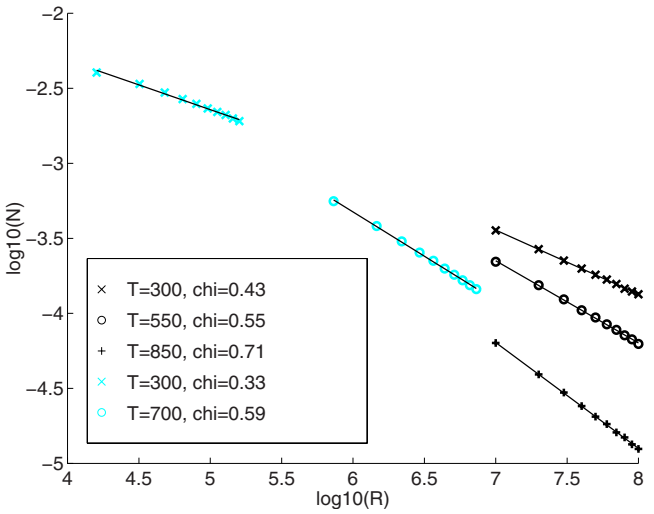

FIG. 5. (Color online) The simulated island density at 10% coverage as a function of $R=D_1/F$, using the test points indicated in Fig. 4. The negative of the gradients of the lines fitted through the sets of data points ("chi") are given in the legend.

The gradients in Fig. 5 are summarized in Table II alongside these predictions. As can be seen, the predictions hold up rather well given the nature of the approximations made in deriving Fig. 4. The $i=8$ regime is perhaps the most difficult to test, since the predicted island density is very low making the Monte Carlo simulation very time consuming and limiting the number of islands nucleated even on a 2000×2000 lattice.

The kinetic phase diagram developed here can be contrasted with the one presented in earlier work where the regimes were predicted from a brute-force numerical integration of rate equations. In fact, the data analysis used there overlooked the unique growth exponent of 2/5 predicted in the dimer-mobility regime and so is in error. In addition, the higher-i regimes were finely divided in that work by simple application of Eq. (4). However, this again is probably oversimplistic since we do not expect sharp thresholds between the regimes as already mentioned. The errors and simplifications evident in our earlier numerical work highlight the advantages of seeking analytical expressions for the structure of the kinetic phase diagram, which enforces more rigor and deepens understanding.

In Fig. 4, we also mark points of interest drawn from Ref. 31, where Furman *et al.* analyzed simulation data in comparison with experiment. Experimental growth of Cu/Cu(100) homoepitaxy had been performed at a deposition rate of 3.21×10^{-4} ML/s, at temperatures $T=213,223,263$ K,[31,32] as indicated by the circles in Fig. 4. Their simulations reproduce well the density variations observed at 30% coverage,[31] and so the simulation data were used with confidence to analyze the scaling behavior at the lower coverage of 10% before island coalescence effects affect the results. The results reported in Table II of Ref. 31 indicate that dimer mobility dominates the island nucleation and growth at $T=263$ K, whereas at the lower temperatures of 213 and 223 K, the $i=1$ growth exponent of 1/3 is obtained. This agrees extremely well with the position of our boundary between these regimes in Fig. 4. It would be interesting to see further experimental tests of our kinetic phase diagram.

TABLE II. The growth exponents for density N_F at various temperature and deposition rates.

Temperature T (K)	Deposition Rate F (ML/s)	Predicted exponent	Measured exponent
300	$(0.331-3.31)\times10^{-1}$	1/3	0.33
300	$(0.529-5.29)\times10^{-4}$	2/5	0.43
550	0.650–6.50	3/5	0.55
700	$(0.100-1.00)\times10^{3}$	3/5	0.59
850	$(0.351-3.51)\times10^{2}$	8/10	0.71

In summary, we have presented a simple Monte Carlo simulation of island nucleation and growth during vapor deposition that allows for the small-island dynamics of diffusion and dissociation. The nucleation and growth have been analyzed in terms of mean field rate equations, and a kinetic phase diagram developed that shows which growth mechanism dominates at various deposition rates and growth temperatures. It should be noted that we have assumed throughout that islands of size $s>8$ will be immobile and stable, whereas in practice they too will have activation energies for diffusion and dissociation.[3] The $i=8$ region on the kinetic phase diagram of Fig. 4 might, therefore, be further divided into $i>8$ regimes. While the work has been presented using modeling data for Cu/Cu(100) island dynamics, the methodology can, in principle, be used for other growth systems. The approach developed here has the advantage of elucidating the functional form of the diagram, rather than relying on brute-force numerical integration of the equations, and so can provide deeper insight into growth mechanisms.

This work has been supported by the UK's Engineering and Physical Sciences Research Council Grant No. GR/T18738/01.

[1] M. Zinke-Allmang, Thin Solid Films **346**, 1 (1999).

[2] For example, see *Atomistic Aspects of Epitaxial Growth*, NATO, Science Series II: Mathematics, Physics, and Chemistry Vol. 65, edited by M. Kotrla, N. I. Papanicolaou, D. D. Vvedensky and L. T. Wille (Kluwer International, London, 2002).

[3] M. Basham, F. Montalenti and P. A. Mulheran, Phys. Rev. B **73**, 045422 (2006).

[4] A.-L. Barabasi and H. E. Stanley, *Fractal Concepts in Surface Growth* (Cambridge University Press, 1995).

[5] J. W. Evans and M. C. Bartelt, Phys. Rev. B **63**, 235408 (2001).

[6] M. C. Bartelt and J. W. Evans, Phys. Rev. B **46**, 12675 (1992).
[7] J. G. Amar, F. Family, and P.-M. Lam, Phys. Rev. B **50**, 8781 (1994).
[8] P. Jensen, A. L. Barabasi, H. Larralde, S. Havlin and H. E. Stanley, Phys. Rev. B **50**, 15316 (1994).
[9] C. Ratsch, A. Zangwill, P. Šmilauer, and D. D. Vvedensky, Phys. Rev. Lett. **72**, 3194 (1994).
[10] J. G. Amar and F. Family, Phys. Rev. Lett. **74**, 2066 (1995).
[11] J. A. Venables, Philos. Mag. **27**, 697 (1973).
[12] V. I. Trofimov and V. A. Osadchenko, *Growth and Morphology of Thin Films* (Energoatomizdat, Moscow, 1993) (in Russian).
[13] G. S. Bales and D. C. Chrzan, Phys. Rev. B **50**, 6057 (1994).
[14] P. A. Mulheran and J. A. Blackman, Phys. Rev. B **53**, 10261 (1996).
[15] P. A. Mulheran and D. A. Robbie, Phys. Rev. B **64**, 115402 (2001).
[16] P. A. Mulheran and D. A. Robbie, Europhys. Lett. **49**, 617 (2000).
[17] P. A. Mulheran, Europhys. Lett. **65**, 379 (2004).
[18] J. G. Amar, M. N. Popescu, and F. Family, Phys. Rev. Lett. **86**, 3092 (2001).
[19] M. C. Bartelt, S. Gunther, E. Kopatzki, R. J. Behm and J. W. Evans, Phys. Rev. B **53**, 4099 (1996).
[20] A. F. Voter, F. Montalenti, and T. C. Germann, Annu. Rev. Mater. Res. **32**, 321 (2002).
[21] G. Henkelman and H. Jónsson, J. Chem. Phys. **111**, 7010 (1999).
[22] G. Henkelman and H. Jonsson, Phys. Rev. Lett. **90**, 116101 (2003).
[23] A. F. Voter, Phys. Rev. B **57**, R13985 (1998).
[24] O. Trushin, A. Karim, A. Kara, and T. S. Rahman, Phys. Rev. B **72**, 115401 (2005).
[25] W. W. Pai, A. K. Swan, Z. Zhang, and J. F. Wendelken, Phys. Rev. Lett. **79**, 3210 (1997).
[26] O. S. Trushin, P. Salo and T. Ala-Nissila, Phys. Rev. B **62**, 1611 (2000).
[27] P. Salo, J. Hirvonen, I. T. Koponen, O. S. Trushin, J. Heinonen, and T. Ala-Nissila, Phys. Rev. B **64**, 161405(R) (2001).
[28] Z.-P. Shi, Z. Zhang, A. K. Swan, and J. F. Wendelken, Phys. Rev. Lett. **76**, 4927 (1996).
[29] K. Kyuno and G. Ehrlich, Phys. Rev. Lett. **84**, 2658 (2000).
[30] J. A. Blackman and P. A. Mulheran, *Electronic, Optoelectronic and Magnetic Thin Films*, edited by J. M. Marshall, N. Kirov, and A. Vavrek (Research Studies, Taunton, UK 1995), p. 227.
[31] I. Furman, O. Biham, J.-K. Zuo, A. K. Swan, and J. F. Wendelken, Phys. Rev. B **62**, R10649 (2000).
[32] A. K. Swan, Z.-P. Shi, J. F. Wendelken and Z. Zhang, Surf. Sci. **391**, L1205 (1997).